Neuronal Silencing and Protection in a Mouse Model of Demyelination

Aniruddha Das,[1, †] Julie Borovicka,[1, †] Hale Tobin,[1] Shruti Bhatia,[1] Jacob Icardi,[1] Ghazaal Tahmasebi,[1] Priyanka Agochiya,[1] Shriya Singh,[1] Bruce Trapp[1] and Hod Dana[1,2]

[†]These authors contributed equally to this work.

1 Department of Neurosciences, Lerner Research Institute, Cleveland Clinic Foundation, Cleveland, OH 44195, USA

2 Department of Molecular Medicine, Cleveland Clinic Lerner College of Medicine of Case Western Reserve University School of Medicine, Cleveland, OH 44195, USA

Correspondence to: Hod Dana

Department of Neurosciences, Lerner Research Institute

Cleveland Clinic Foundation, Cleveland, OH 44195, USA

e-mail danah@ccf.org

Keywords: Cuprizone model; calcium imaging; two-photon microscopy; third-harmonic generation microscopy; Clemastine Fumarate.

Abstract

Damage to the myelin sheath that protects axons in the central nervous system is a hallmark pathology of demyelinating diseases like multiple sclerosis. Cuprizone-induced demyelination in mice is a common model for studying demyelination and remyelination. However, the relationship between myelin damage and recovery and the functional properties of ensheathed neurons remains poorly understood. Using concurrent monitoring of hippocampal myelination and neuronal firing rates in the same mouse, we assessed longitudinal changes during cuprizone consumption and remyelination treatment. The data revealed a rapid decline in neuronal activity that preceded myelin loss. Females showed a more severe decrease after 4 days of cuprizone, which correlated with enhanced neuronal activity and myelin loss 51 days later, whereas male mice showed a more severe decline in neuronal activity after 55 days of cuprizone. Following cuprizone cessation, mice were treated with Clemastine or vehicle for 45 days. A short-term recovery was found in both groups, before the Clemastine group showed increased remyelination and higher neuronal firing rates. The mean increase and decrease in firing rates were proportional to the same-neuron baseline

firing rate in the Clemastine and vehicle groups, respectively, highlighting a potential linkage between the status of myelin recovery and cellular activity.

Introduction

Myelin is a multi-layered sheath that is produced by oligodendrocytes, insulates axons, and enables the rapid transmission of action potentials.[1] In demyelinating diseases like multiple sclerosis (MS), myelin degeneration leads to severe symptoms, including speech, motor, and visual deficits, along with long-term cognitive decline.[2,3] Cognitive and memory loss in MS patients are linked to hippocampal demyelination and atrophy.[2,4] While MS is recognized as a disease with a major autoimmune inflammatory component, basic studies, human tissue biopsies, and patient autopsies suggest that primary oligodendrocyte dystrophy also contributes to its development.[5,6]

Rigorous study of demyelination-related pathologies requires the use of an appropriate animal model, especially since patient tissue is usually limited to the late stages of the disease.[7] Such an established model is the mouse cuprizone model.[8] Cuprizone is a copper chelator, which induces selective death of mature oligodendrocytes in the brain, leading to extensive demyelination including in the hippocampus. Additionally, this model allows studying remyelination processes that occur spontaneously after cessation of cuprizone consumption.[8,9] Previous studies showed gradual brain-wide demyelination that typically begins 2-3 weeks after cuprizone initiation and continues as long as it is consumed.[10]

Previous reports have found that cuprizone-induced hippocampal demyelination alters CA1 neuronal function and long-term potentiation in tissue slices.[4,11] We found reduction of hippocampal neuronal firing *in vivo* during cuprizone consumption, with partial recovery upon returning to regular diet.[12] Partial remyelination was shown to be sufficient to restore cortical function following therapeutically enhanced oligodendrogenesis.[13] However, the relationship between re/demyelination and neuronal functionality is yet poorly understood.

In this study, we longitudinally recorded two-photon laser scanning microscopy (TPLSM) fluorescence from CA1 neurons of transgenic mice expressing the jRGECO1a calcium sensor to monitor their firing rates (FRs).[14,15] Concurrently, we recorded third-harmonic generation (THG) signals from the same mice. THG produces label-free signals from areas rich in lipids, like myelin, that enables monitoring their myelination status.[16,17] Upon cuprizone consumption, we found a rapid reduction in neuronal FRs alongside gradual demyelination. Male and female mice showed

different neuronal activity reduction patterns, and correlation between neuronal activity reduction and myelin loss were found for females only. Following cuprizone cessation, mice were treated with Clemastine, a drug under clinical trial for MS patients, to enhance remyelination.[18,19] This treatment also restored neuronal FR levels to their pre-cuprizone levels.

Materials and methods

All surgical and experimental procedures were conducted in compliance with protocols approved by the Institutional Animal Care and Use Committee and Institutional Biosafety Committee of the Lerner Research Institute. ARRIVE guidelines were used to report findings.[20]

Surgical procedures

Thy1-jRGECO1a mice (10-12 weeks old) were implanted with hippocampal windows above their left hippocampus as previously published.[15,21,22] Briefly, mice were anesthetized using isoflurane (3% for induction, 1.5% during surgery), the scalp skin was removed, and a craniotomy (3.2mm diameter) was drilled (-2/-2 AP/ML from Bregma, OMNIDRILL35, WPI). The tissue above the hippocampus was aspirated, while leaving it intact. A glass coverslip (3mm diameter #1 glass, Warner Instruments) attached to a metal cannula (2.65/3.2mm internal/outer diameters, 1.8mm length, New England Small Tube, 304L stainless steel) was placed above the hippocampus. The cannula and a headbar were secured to the skull using dental cement (Contemporary Ortho-Jet) and a cyanoacrylate glue.

Longitudinal recordings

Mice were intramuscularly injected with Chloroprothixene Hydrochloride (30µl of 0.33mg/ml, Spectram Chemical) and were kept on a 37°C heating pad under light anesthesia (0.5-0.75% isoflurane).[12] TPLSM was used to record spontaneous activity of CA1 pyramidal neurons expressing jRGECO1a using 1100 nm excitation light (100-200mW, Insight X3, Spectra-Physics), using a 10x 0.5NA objective (Bergamo II microscope, Thorlabs; resonant/galvo scanners, 512x512 pixels, 600x600µm^2, 30frames/sec, 607/70nm emission filter, Semrock). 3-5 fields of view (FOVs) were typically collected for 200 seconds each. 1-2 baseline recordings were conducted before the initiation of cuprizone diet, and on cuprizone days (CDs) 4, 18, 32, 46, and 55. Then, on treatment days (TDs) 3, 6, 10, 13, 17, 25, 35, and 45. All recording sessions were identical. For some of the mice, the same FOVs and neurons were re-located every session.

THG recordings were conducted using the same microscope and 1260 nm excitation wavelength (15-60 mW, Carbide 40W laser and Orpheus-F OPA, Light Conversion. Galvo-galvo

scanners, 1024x1024 pixels, ~1-2 frames/sec with a 434/32nm filter, Semrock). To minimize heat-induced damage risk, recording was conducted for one baseline, and on CDs 18, 32, 46, and 55, and on TDs 6, 13, 25, 35, and 45.

Mouse model of demyelination and remyelination

Mice were kept in standard housing (12-hour light/dark cycle, access to food and water *ad libitum*) and were given 4-7 weeks for post-craniotomy recovery before the recordings were initiated. After initiating the recording of part of the mice, we identified that a minimum recovery period of 40 days is needed for achieving stable CA1 activity and myelin signal. Hence, only mice that had at least one baseline recording after 40 or more days post-craniotomy were included in the study and the rest were excluded (n=24, Supp. Fig. 1). Following the baseline recordings, mice were randomly assigned into two groups. The cuprizone group was fed with 0.3% cuprizone diet (TD. 140805, Envigo), while the control group continued with regular diet. The cuprizone pellets were kept at 4°C and replaced three times/week. Following 55 days of cuprizone diet, the mice resumed on regular diet for 45 additional days until the study's endpoint. Mouse weights were monitored on each recording day.

Following cuprizone diet's cessation, cuprizone group mice were randomly divided into two groups. One group was treated daily in random order with Clemastine (Sigma-Aldrich; 10 mg/kg, oral gavage of 1.33 mg/ml Clemastine Fumarate in 90% H_2O, 5% Tween-20, and 5% DMSO). The second group received identical vehicle solution treatment. Mice that were removed from the study during the cuprizone or treatment phases due to health or window quality concerns, were excluded from the analysis (n=35, Supp table 1). No blinding was used.

Data analysis

Analyses were based upon custom MATLAB scripts (MathWorks), similar to our previous work.[12] Raw fluorescence movies were registered for correcting small movements.[23] Somatic regions of interest (ROIs) were segmented using CellPose.[24] Pixels of each ROI were averaged to calculate the time-dependent fluorescence signal (F). Baseline fluorescence (F_0) was estimated as the median of F. Action potential (AP) number was estimated using the SpikeML algorithm using jRGECO1a parameters.[14,25] Myelin coverage was quantified by applying two thresholds on the raw images using Otsu's method and calculating the ratio of the brightest pixels vs. all pixels. Myelin fiber properties were measured by fitting a Gaussian function to visually-identified same-fibers' cross section across different images. Thickness was defined as the fit's full width at half

maximum (FWHM). The amplitude was defined as the maximum of the fit minus its minimum. All recordings were inspected for quality issues, like movement artifacts and relocation of the same myelinated fibers. In case issues were found, the specific session was excluded (TPLSM recordings: n_1= 9 sessions from n_2= 9 mice; THG recordings: n_1= 22 sessions from n_2= 18 mice, Supp Table 2). Same-cell data were compared across four days: baseline, CD55, TD10, and TD45. The segmented FOVs were compared using a probabilistic model of cell centroid distances to identify the same cells.[26] The same-cell FRs were calculated, and outliers were excluded using the ROUT method (Q = 0.01). Separately, cells which were identified just in the [baseline, TD10, and TD45] or [baseline, CD55 and TD10] datasets, were also excluded of outliers (ROUT, Q = 0.01) and binned into partially-overlapping bins of +/- 0.025 Hz baseline FRs. We calculated histograms of change in average FR from TD10 to TD45 or CD55 to TD10 for each bin, which were fitted with scaled Lorentzian functions: $Y = a/(1 + ((x - b)/\gamma)^2)$. Bins with less than 20 cells or R^2 of fit lower than 0.8 were omitted. Linear regressions of the baseline FRs vs. the function's peak and FWHM were calculated.

Statistical analyses

Analyses were conducted using GraphPad Prism (version 10.1.2). FRs and myelin signals were fit with repeated measure ANOVAs or mixed-effect models when there were missing data points. The mixed models used a compound symmetry covariance matrix and were fit using Restricted Maximum Likelihood. In the absence of missing values, this method gives the same *P* values and multiple comparisons tests as repeated measures ANOVA. Data fit was confirmed by checking QQ plot. *Post hoc* comparisons used Dunnett's test to compare with baseline and Tukey's HSD for additional comparisons. Pearson's correlation was used to evaluate relationships between different variables. Mann-Kendall test was used to detect monotonic trends. A significance threshold of $P < 0.05$ was used for all statistical tests. Details on statistical effect sizes may be found in Supplementary Statistical Data.

Results

Longitudinal monitoring of neuronal activity and myelin status

TPLSM and THG were used to record firing of CA1 pyramidal neurons and to monitor their hippocampal myelination status, respectively (Fig. 1A-B). All mice were randomly assigned to two groups. The cuprizone group was fed with 0.3% cuprizone diet for 55 days, followed by 45 days of daily treatment with Clemastine or vehicle (Fig. 1C). The control group was fed with

regular diet for the entire study period and received no treatment. Identical THG and TPLSM recordings were conducted at selected timepoints to monitor longitudinal changes in neuronal activity, myelin condition, and body weight (Fig. 1D-F, Supplementary. Fig. 2).

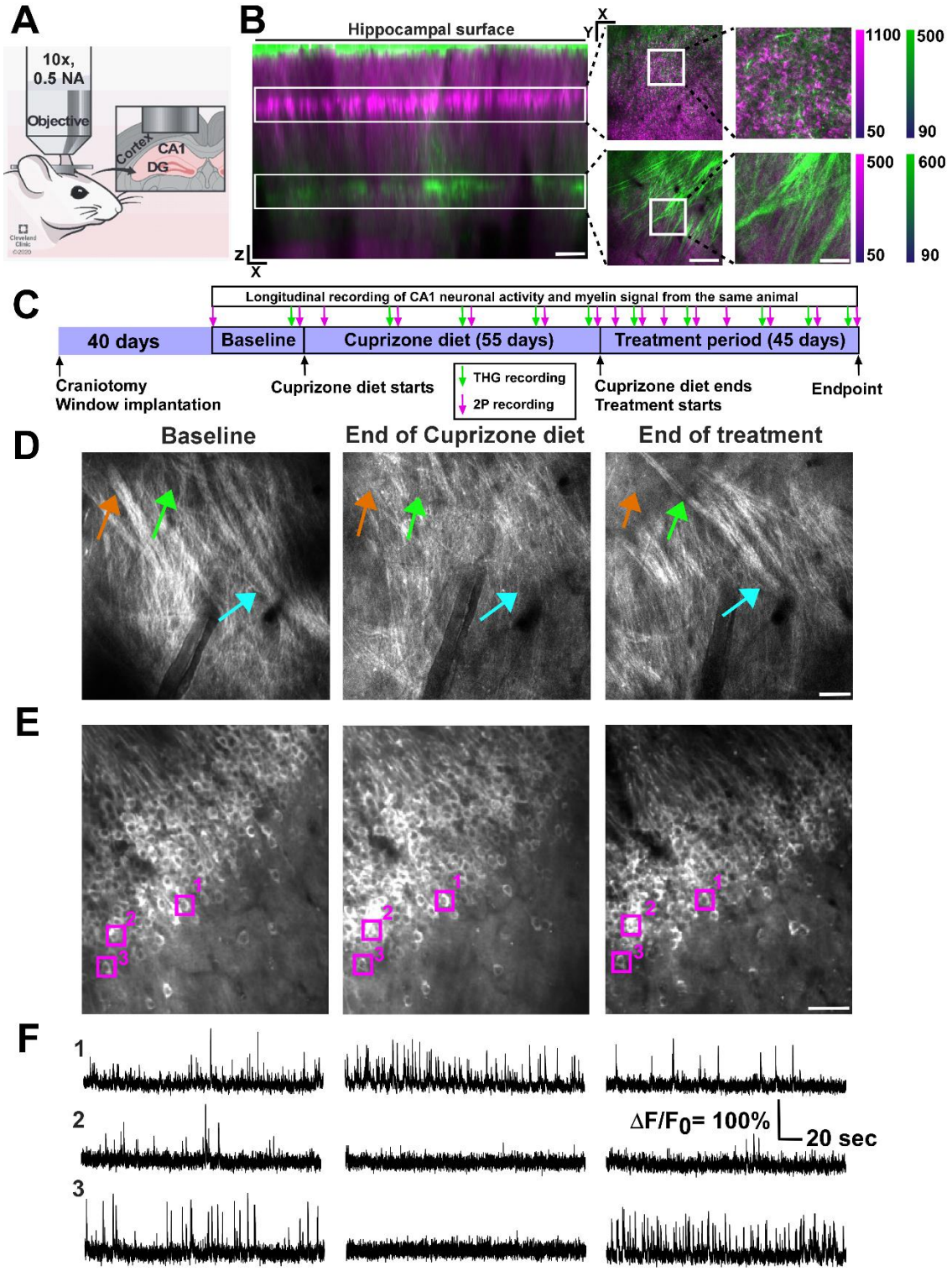

Figure 1: Longitudinal monitoring of hippocampal CA1 activity and myelination levels in a mouse model of de/remyelination. (A) Illustration of hippocampal window implantation to allow long-term access to the hippocampus of a Thy1-jRGECO1a mouse. **(B)** *In vivo* side view (scale bar=75µm) of a Thy1-jRGECO1a hippocampus shows CA1 neurons, axons, and dendrites expressing the red calcium sensor jRGECO1a (acquired by TPLSM and shown in magenta) and hippocampal myelin (acquired by THG and shown in green). Insets: horizontal views of the CA1 and thick myelinated fiber layers (scale bar for the left and right images are 200 and 50µm, respectively. **(C)** Timeline for neuronal activity and myelin recording sessions (indicated by magenta and green arrows, respectively). These timings are designed to capture the baseline, early, intermediate, and late phases of the cuprizone diet and treatment periods. **(D)** Example THG images from the same FOV (scale bar=50µm) show the disappearance (at Cuprizone Day 55, orange and cyan arrows), reappearance (cyan arrows), and newly-appearing myelin fibers (green arrows) during the cuprizone consumption and recovery periods. **(E)** Example TPLSM images from the same FOV of CA1 neurons (scale bar=50µm) expressing jRGECO1a. The same cells are highlighted by the numbered magenta squares in the different images. **(F)** Raw fluorescence traces of the cells shown in E. Firing of action potentials causes an increase in the fluorescence signal.

Sex-specific patterns of CA1 activity loss during cuprizone consumption

Following cuprizone consumption, the myelin signal gradually and significantly decreased from baseline levels, without significant sex differences (Fig. 2A). The neuronal FR significantly decreased from baseline activity levels after 4 days of cuprizone diet and remained significantly lower than baseline for the entire 55 cuprizone diet days. Female mice showed significantly lower CA1 FRs than males on day 4. Then, CA1 FRs slightly recovered and where comparable for both sexes in days 18-32. Finally, a second decrease was detected in days 46-55, which was more severe in male mice and led to significantly lower FRs in males on CD55 (Fig. 2B).

Correlated brain activity and demyelination levels during cuprizone consumption

We assessed whether the rapid decrease in FR from baseline to CD4 was correlated with FR levels on other recording days. We found significant positive correlations for female mice on recording days 32, 46, and 55, but no significant correlations for males (Fig. 2C-D). Moreover, there was a significant correlation between the same-female percent loss of CA1 activity on CD55 and the percent of myelin signal loss on the same day (Fig. 2E), but not in males. Finally, a significant correlation was also found between same-female loss of CA1 activity on CD4 and the loss of myelin on CD55, which was also not observed in males (Fig. 2F).

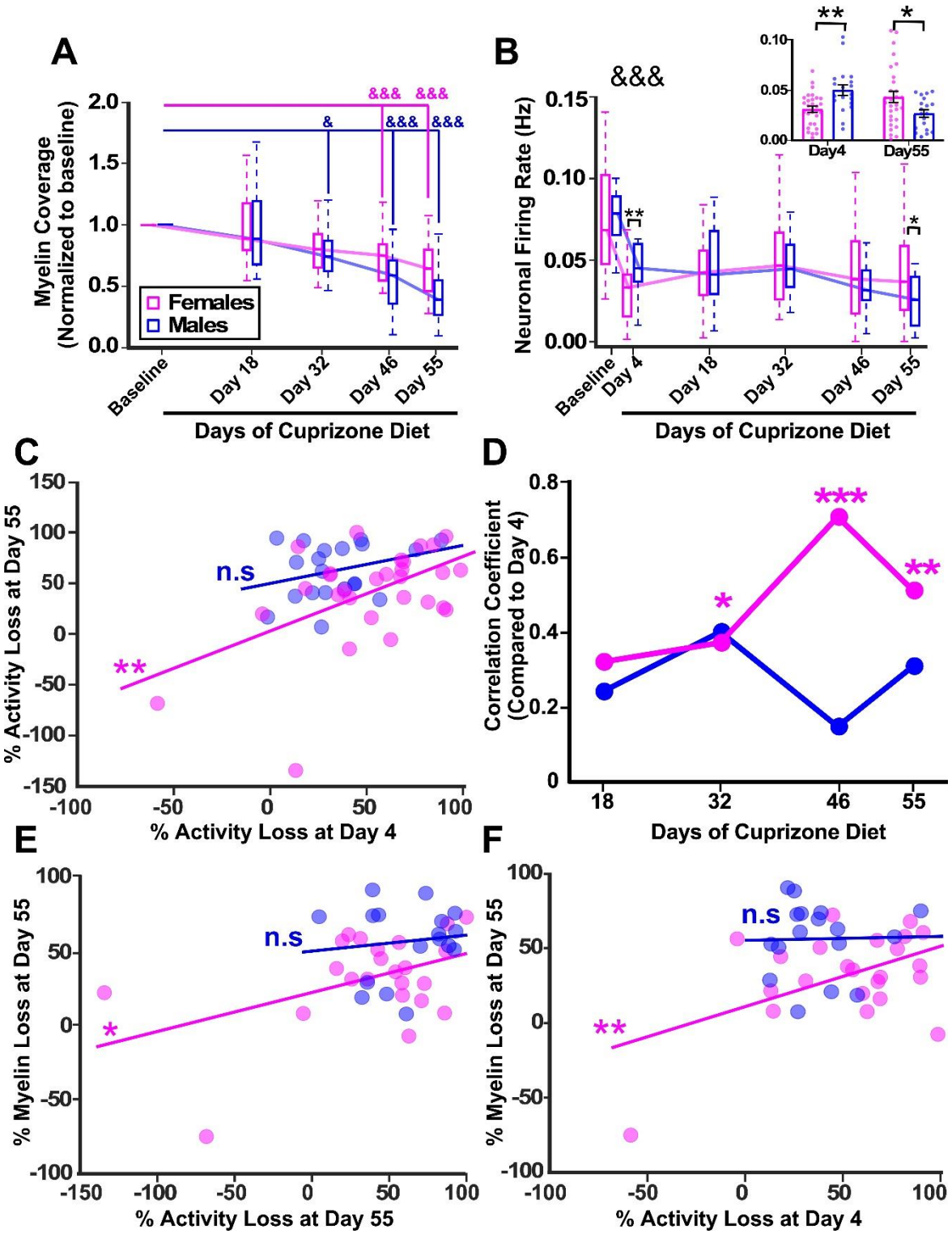

Figure 2: Loss of brain activity and correlations between cuprizone-induced functional and morphological pathologies are sex-specific. (A) Myelin coverage gradually decreased for cuprizone male and female mice without sex differences. Myelin coverage values were normalized to the same-mouse baseline levels. (*n*=43, 17 males and 26 females; linear mixed-effect model with Dunnett's *post hoc* comparisons, &, *P*<0.05, &&&, *P*<0.001). Boxplots show medians and 25-75 quartiles, and the whisker length is the shorter of 1.5 times the inter-quartiles range or the extreme

data point. Outliers are not shown. **(B)** CA1 FRs showed significant reduction 4 days after cuprizone diet initiation for both males and females, with a significantly larger decrease in females. Following a slight recovery on days 18-32, a second decline was detected between CDs 46-55, resulting in a significantly lower FR in males on CD55 (n=48 mice, 19 males and 29 females; females: 250-3525 neurons/mouse, median=1083 neurons; males: 158-3207 neurons/mouse, median 1178 neurons; linear mixed-effect model with Tukey's HSD. Inset shows individual mouse data points and the group average and SE on CDs 4 and 55 (P=0.0036 and 0.018 respectively). &&&, P<0.001 for time effect; *, P<0.05, **, P<0.01 for sex differences. **(C)** Same-mouse reduction of CA1 FR (%) from baseline to CD4 vs. from baseline to CD55 showed significant correlations among females, but not males (r=0.51 and P=0.0047 for females and r=0.31 and P=0.20 for males; Pearson's correlation was used for all tests in C-F. The correlation coefficient *(r)* and significance *(P)* are reported). **(D)** Summary of the Pearson's r value for % FR reduction from baseline to CD4 vs. from baseline to all other cuprizone recording days. *, P<0.05; **, P<0.01; ***, P<0.001. **(E)** Same-mouse reduced CA1 FR (%) and the loss of myelin coverage (%) from baseline to CD55 are correlated for female mice (r =0.45, P=0.033), but not for males (r =0.12, P=0.65). **(F)** Same-mouse reduced CA1 FR (%) from baseline to CD4 and the loss of myelin coverage (%) from baseline to CD55 are also correlated for female mice (r =0.49, P=0.018), but not for male mice (r =0.02, P=0.93). Additional details may be found in Supplementary Statistical Data.

Clemastine remyelination treatment restores CA1 firing rates

Following 55 days of cuprizone diet, mice in the cuprizone group were switched to regular diet and were randomly assigned into two groups. The Clemastine group received daily oral gavage treatment of Clemastine for 45 days, and the vehicle group received vehicle solution only. In agreement with previous studies, Clemastine-treated mice showed increased remyelination compared to vehicle-treated mice, as measured by the increased myelin coverage, and myelinated fibers' signal amplitude and thickness (Fig. 3A-C). For the first 6 days after cuprizone cessation, there was a small increase in myelination coverage in both groups. Then, the vehicle group showed a monotonous decrease and the Clemastine group showed a monotonous increase for the following days (Fig. 3D). A similar trend was evident with CA1 FR, when a short-term increase was measured in both group for the first 6 treatment days, followed by a monotonous decrease in the vehicle group and a gradual increase in the Clemastine group. These different patterns led to a significant effect of the Clemastine treatment on CA1 activity levels (Fig. 3E). No significant changes were found in the FR and myelination of the control group (Supplementary Fig. 3). Comparison with proteolipid-protein-stained samples, which were collected at the study endpoint, showed non-significantly higher myelin coverage in the control, then in the Clemastine, and the lowest in the vehicle group (Supplementary Fig. 4).

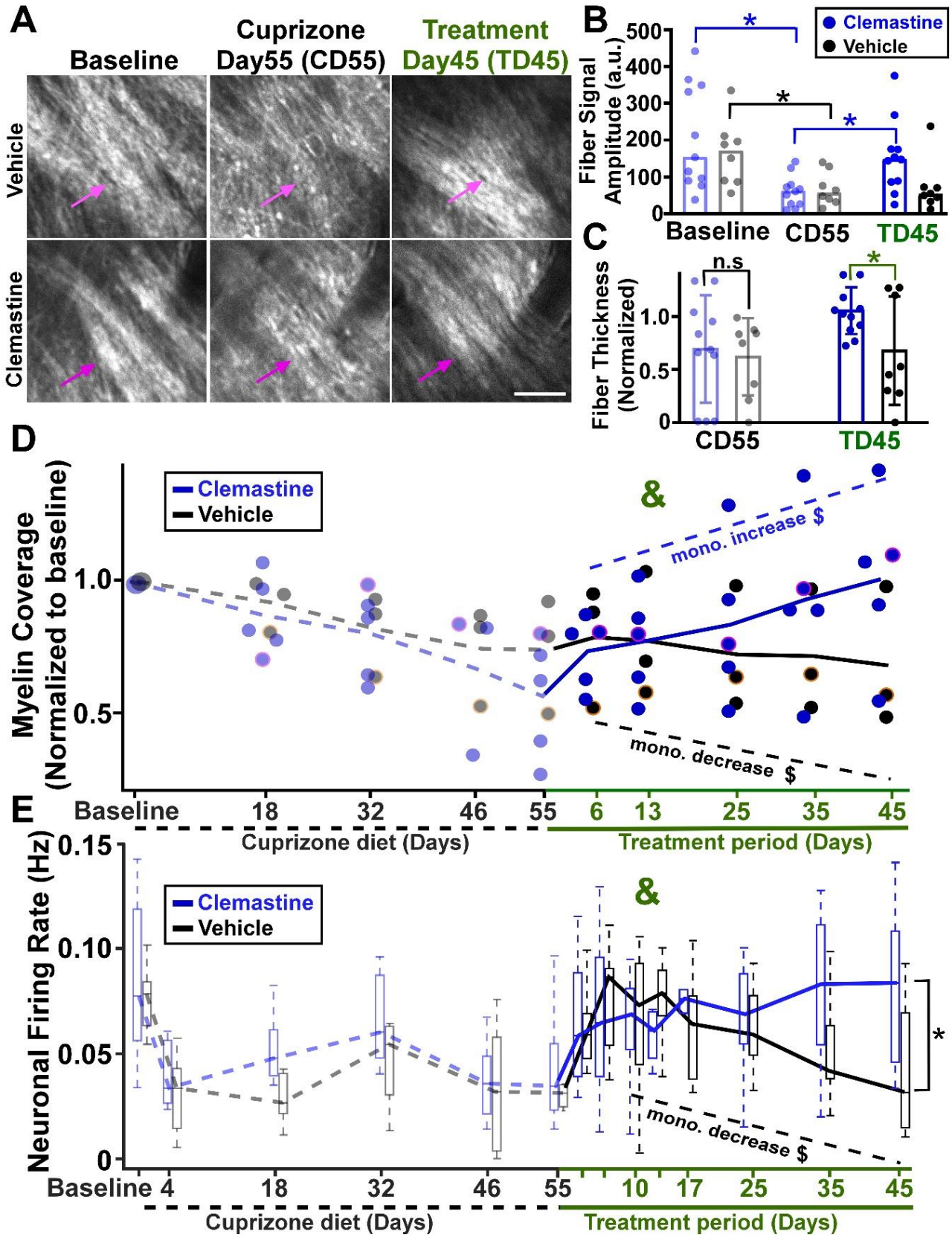
A
Baseline
Cuprizone Day55 (CD55)
Treatment Day45 (TD45)
Vehicle
Clemastine
B
Clemastine
Vehicle
Fiber Signal Amplitude (a.u.)
500
400
300
200
100
0
*
*
*
Baseline
CD55
TD45
C
Fiber Thickness (Normalized)
1.0
0.5
0
n.s
*
CD55
TD45
D
Clemastine
Vehicle
Myelin Coverage (Normalized to baseline)
1.0
0.5
&
mono. increase $
mono. decrease $
Baseline
18
32
46
55
6
13
25
35
45
Cuprizone diet (Days)
Treatment period (Days)
E
Neuronal Firing Rate (Hz)
0.15
0.10
0.05
0
Clemastine
Vehicle
&
*
mono. decrease $
Baseline
4
18
32
46
55
10
17
25
35
45
Cuprizone diet (Days)
Treatment period (Days)

Figure 3: Clemastine treatment restores brain activity levels. (A) THG images of the same FOV from the same mice on baseline, CD55 and TD 45. Arrows indicate the location of the same fibers in the different images (upper row: vehicle-treated mouse, bottom row: Clemastine-treated mouse; all images are contrast-enhanced; scale bar=50µm). **(B-C)** Cross-sections of individual fibers (example fibers shown in A) were fit with a Gaussian function to estimate the fiber amplitude over its surrounding background (**B**) and thickness normalized to same-fiber baseline values (**C**; Clemastine group: n_1=5 mice, n_2=11 same-fibers; vehicle group: n_1=3 mice, n_2=8 same-fibers). Until CD55 both groups were under the same conditions, and the fiber properties were similar, with significant decrease in the fiber thickness and amplitude due to cuprizone-induced demyelination. Clemastine treatment caused a significant fiber thickness and amplitude increase, which was not apparent in the vehicle group (Fiber signal amplitude: two-way ANOVA with HSD, Clemastine group: baseline vs. CD55, *P*=0.019, CD55 vs. TD45, *P*=0.037; vehicle group: baseline vs. CD55, *P*=0.017. Fiber thickness: Clemastine vs. vehicle on CD55, *P*=0.73, and on TD45, *P*=0.043, unpaired student t-test). (**D**) Both the vehicle and Clemastine groups (*n*=8 mice, five Clemastine and three vehicle) showed a mean myelin coverage increase during the first 6 days of treatment. From TD6 to the study endpoint, the mean myelin coverage of the Clemastine-treated mice monotonously increased, while it monotonously decreased for the vehicle-treated mice, leading to a significant difference at the study endpoint (*P*=0.028 for monotonous trends in both groups, Mann-Kendall test, marked by $. Two-way ANOVA analysis of TD6 to TD45 data showed a significant interaction between time and group, *P*=0.038, marked by &, without significant *post-hoc* differences). Each dot shows data from one mouse; pale and dotted lines connect the means during the cuprizone diet period and dark and solid lines during the treatment period. Dots with magenta/orange borders show data from the respective Clemastine/vehicle images in A. **(E)** Clemastine treatment enhanced the mean CA1 FR compared to vehicle (*n*=15 mice, eight Clemastine and seven vehicle; Clemastine: 321-3207 neurons/mouse, median 985 neurons; vehicle: 250-3021 neurons/mouse, median 915 neurons). Same-mouse CA1 FR was longitudinally recorded during the cuprizone diet period (pale and dotted lines and boxplots), and the treatment period (dark and solid lines and boxplots). During the first 6 days of the treatment period, the CA1 FRs in both groups increased. From TD10 until the study endpoint, the vehicle group mean FR monotonously decreased (*P*=0.024, Mann-Kendall test, marked by $). This trend was not evident in the Clemastine group, which exhibited a stable recovery back to baseline FR levels. On TD45, the Clemastine- and vehicle-treated groups exhibited a significant difference in FR (*P*=0.049 for Clemastine vs. vehicle on TD45; *P*=0.033 for interactions between time and group; linear mixed-effect model with HSD). Boxplots show medians and 25-75 quartiles, and the whisker length is the shorter of 1.5 times the inter-quartiles range or the extreme data point. Outliers are not shown. Additional details may be found in Supplementary Statistical Data.

Cellular-level responses to treatment

In a subset of the cuprizone group, the same neurons were monitored throughout the entire study period. Same-cell activity was compared between baseline, CD55, TD10, and TD45 (Fig. 4A). We checked whether the neuronal baseline FR was correlated with the early and late recovery patterns that were identified (Fig. 3E). Between CD55 and TD10, the change in FR of Clemastine neurons showed no dependency on their baseline FR. However, for vehicle neurons, a positive correlation with the baseline FR was found, indicating that cells with high baseline FR showed larger increases on average between CD55 and TD10 (Supplementary Fig. 5). Interestingly, between TD10 and TD45 the effect of treatment has the opposite correlation with same-cell baseline FR for each group. For Clemastine neurons, a higher baseline FR was correlated with a higher mean FR increase, while for vehicle neurons it was correlated with a bigger decrease (Fig. 4E). Finally, the variability of the mean increase/decrease in FR also increased with the baseline FR (Fig. 4F).

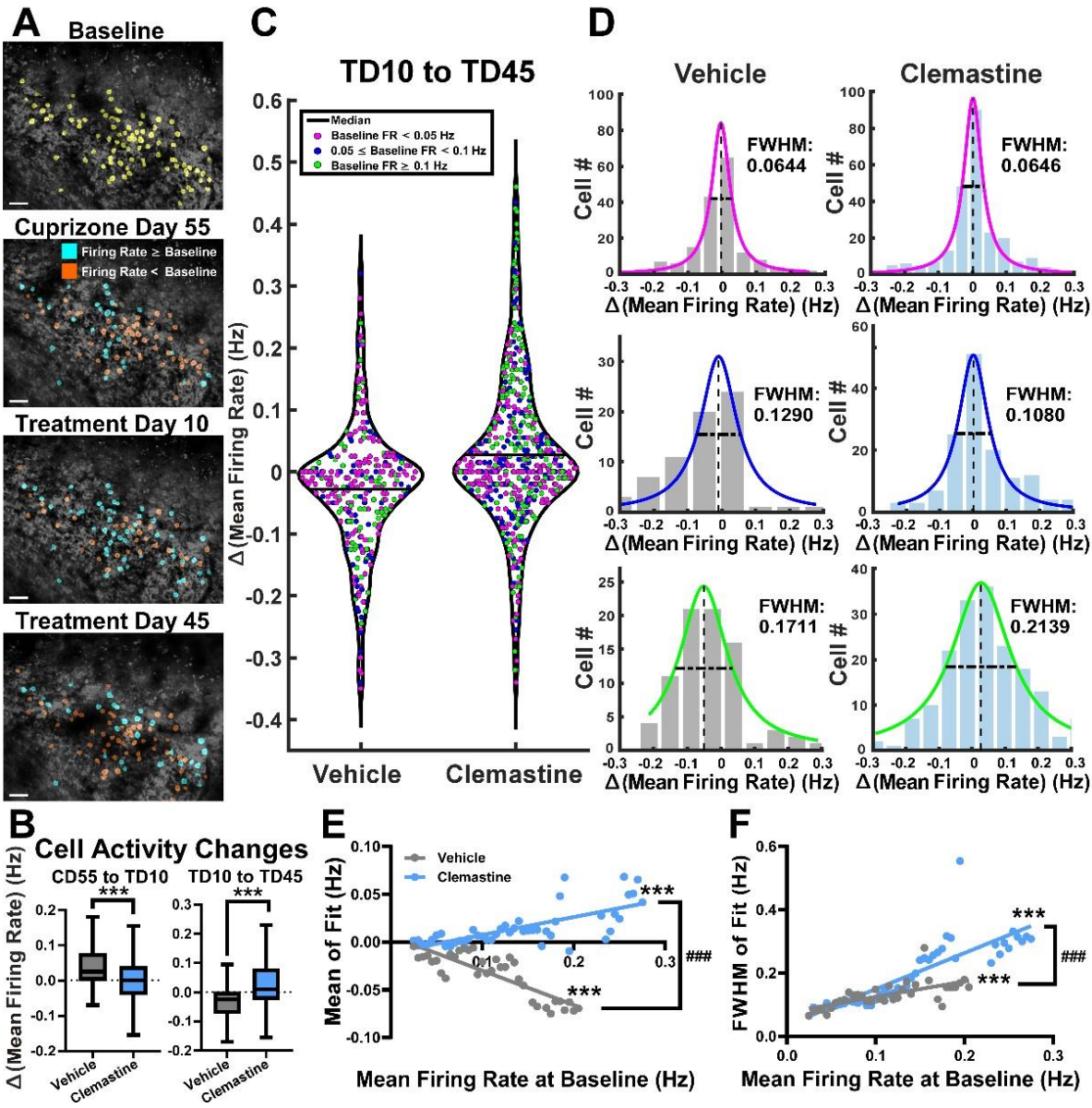

Figure 4: Single-cell correlates of recovery during Clemastine treatment. (A) Example FOV shows tracking of the same cells in a vehicle mouse (*n*=87 cells, shown in yellow in the baseline image) across baseline, CD55, TD10, and TD45 recording days. Cyan-labeled cells exhibited equal or higher FR than their baseline levels, while orange-labeled cells exhibited lower FR than their baseline FR. **(B)** Distributions of the same-cell changes of FR from CD55 to TD10 (left) and from TD10 to TD45 (right) for the vehicle and Clemastine groups (*n*=6, 3 mice per group, with 165 and 336 same-cells in the vehicle and Clemastine groups, respectively). Similar to the population-level data (Fig. 3), the vehicle group showed a significantly higher increase between CD55 to TD10 than the Clemastine group (*P*<0.0001, unpaired Student's t-test), followed by a decrease from TD10 to TD45. The Clemastine group showed an increase between TD10 to TD45, which was significantly higher than the vehicle group (*P*<0.0001, unpaired Student's t-test). **(C)** Violin plot of the change in same-cell FR between TD10 to TD45, where the color of each dot indicates whether the baseline FR of the cell was high, medium, or low (*n*=306 and 553 cells from vehicle and Clemastine groups, respectively). **(D)** Individual data points from C were grouped into histograms of low-, medium-, and high-baseline FR cells, and each histogram was fitted with a Lorentzian function. The data show that cells with increased baseline FRs tend to have larger FWHM values. Moreover, the mean change of high-activity neurons in the Clemastine group was positive, while

for the vehicle group it was negative. **(E)** The same cells from Panel C were grouped into partially-overlapping bins based upon their baseline FRs. Histograms of the FR changes from TD10 to TD45 for each bin were fitted with Lorentzian functions, as shown in D, and the fits' mean and FWHM are shown. The mean change in the FR between TD10 to TD45 was linearly correlated with the same-cell baseline FR in the Clemastine group and was negatively correlated with the same-cell baseline FR in the vehicle group (Clemastine, r=0.7024, vehicle, r= -0.8451; P<0.001 for both groups, Pearson's correlation). **(F)** Both groups showed an increase in variability, as reflected by increased FWHM, with the increase of same-cell baseline FR (Clemastine, r=0.8436, vehicle, r=0.6602; P<0.001 for both groups). ***, P<0.001 significance of Pearson correlation; ###, P<0.001, significance of ANCOVA test for checking significant difference in the fit lines' slopes.

Discussion

This work presents a novel *in vivo* approach to longitudinally measure both brain activity and myelination of axons from the same animal throughout toxin-induced demyelination and remyelination treatment. It was shown that neuronal activation promotes myelination via oligodendrogenesis in the mouse brain.[27] This study identifies that for the cuprizone model of demyelination, loss of brain activity precedes the loss of myelin and that functional decrease on CD4 predicts the same mouse morphological decay on CD55 (Fig. 2).

We found sex-specific differences in the measured brain activity patterns. Female mice showed a more severe decline in CA1 activity within 4 days of cuprizone consumption, while males exhibited a more severe decline after 55 days of cuprizone. For female mice, but not for males, the correlations of the FR loss with CD4 increased over time (Fig. 2D-E). This suggests that the severity of cuprizone-induced neuronal silencing is largely maintained throughout the 55 days of cuprizone consumption. Notably, Females are predisposed to MS relapses more than males[28], which makes demyelination-related sex-differences a question with potential translational directions. These findings suggest that neuronal activity recording reveals some of the underlying sex differences that are not apparent by recording myelin condition alone.

Remyelination therapy may alleviate the condition of MS patients, especially during progressive stages of the disease.[29] Clemastine enhances myelin repair (Fig. 3B-D), presumably by enhancing the maturation of myelinating oligodendrocytes.[30] Our findings demonstrate that it also significantly restored neuronal FR compared to vehicle-treated mice to levels close to baseline FRs (Fig. 3E). Therefore, Clemastine's neuroprotective effect extends beyond regenerating myelin only; it also protected the neuronal activity that may have further declined due to the cuprizone consumption. Moreover, Clemastine's treatment was showed to increase the FR of individual neurons in a proportional manner to their baseline FR. The effect was opposite to neurons in the vehicle group (Fig. 4E). This suggests that the neuroprotective effect of Clemastine interacts with

intrinsic cellular properties, such as the baseline FR, and may have additional cell-specific characteristics that are yet to be found.

Data availability

Data related to this study will be available from the corresponding author upon request.

Acknowledgements

The authors would like to thank Drs. Christopher Nelson and Xuefeng (Chris) Liu for helpful comments and suggestions, as well as to Drs. Monica Boyle, Kevin Dines, and Mrs. Iliana Ruiz for input on the study design.

Competing interests

The authors declare no competing interests.

References

1. Stadelmann C, Timmler S, Barrantes-Freer A, Simons M. Myelin in the central nervous system: structure, function, and pathology. *Physiological reviews*. 2019;

2. Geurts JJ, Bö L, Roosendaal SD, *et al*. Extensive hippocampal demyelination in multiple sclerosis. *Journal of Neuropathology & Experimental Neurology*. 2007;66(9):819-827.

3. Huang WJ, Chen WW, Zhang X. Multiple sclerosis: Pathology, diagnosis and treatments. *Experimental and therapeutic medicine*. 2017;13(6):3163-3166.

4. Dutta R, Chang A, Doud MK, *et al*. Demyelination causes synaptic alterations in hippocampi from multiple sclerosis patients. *Annals of neurology*. 2011;69(3):445-454.

5. Lucchinetti C, Brück W, Parisi J, Scheithauer B, Rodriguez M, Lassmann H. Heterogeneity of multiple sclerosis lesions: implications for the pathogenesis of demyelination. *Annals of Neurology: Official Journal of the American Neurological Association and the Child Neurology Society*. 2000;47(6):707-717.

6. Bierhansl L, Hartung H-P, Aktas O, Ruck T, Roden M, Meuth SG. Thinking outside the box: non-canonical targets in multiple sclerosis. *Nature reviews Drug discovery*. 2022;21(8):578-600.

7. Denic A, Johnson AJ, Bieber AJ, Warrington AE, Rodriguez M, Pirko I. The relevance of animal models in multiple sclerosis research. *Pathophysiology*. 2011;18(1):21-29.

8. Vega-Riquer JM, Mendez-Victoriano G, Morales-Luckie RA, Gonzalez-Perez O. Five decades of cuprizone, an updated model to replicate demyelinating diseases. *Current neuropharmacology*. 2019;17(2):129-141.

9. Castillo-Rodriguez MdlA, Gingele S, Schröder L-J, *et al*. Astroglial and oligodendroglial markers in the cuprizone animal model for de-and remyelination. *Histochemistry and cell biology*. 2022;158(1):15-38.

10. Zirngibl M, Assinck P, Sizov A, Caprariello AV, Plemel JR. Oligodendrocyte death and myelin loss in the cuprizone model: an updated overview of the intrinsic and extrinsic causes of cuprizone demyelination. *Molecular neurodegeneration*. 2022;17(1):34.

11. Baltan S, Jawaid SS, Chomyk AM, *et al*. Neuronal hibernation following hippocampal demyelination. *Acta neuropathologica communications*. 2021;9:1-15.

12. Das A, Bastian C, Trestan L, *et al*. Reversible loss of hippocampal function in a mouse model of demyelination/remyelination. *Frontiers in cellular neuroscience*. 2020;13:588.

13. Della-Flora Nunes G, Osso LA, Haynes JA, *et al*. Incomplete remyelination via therapeutically enhanced oligodendrogenesis is sufficient to recover visual cortical function. *Nature Communications*. 2025;16(1):732.

14. Dana H, Mohar B, Sun Y, *et al*. Sensitive red protein calcium indicators for imaging neural activity. *Elife*. 2016;5:e12727.

15. Dana H, Novak O, Guardado-Montesino M, *et al*. Thy1 transgenic mice expressing the red fluorescent calcium indicator jRGECO1a for neuronal population imaging in vivo. *PloS one*. 2018;13(10):e0205444.

16. Farrar MJ, Wise FW, Fetcho JR, Schaffer CB. In vivo imaging of myelin in the vertebrate central nervous system using third harmonic generation microscopy. *Biophysical journal*. 2011;100(5):1362-1371.

17. Weigelin B, Bakker G-J, Friedl P. Third harmonic generation microscopy of cells and tissue organization. *Journal of Cell Science*. 2016;129(2):245-255.

18. Green AJ, Gelfand JM, Cree BA, *et al*. Clemastine fumarate as a remyelinating therapy for multiple sclerosis (ReBUILD): a randomised, controlled, double-blind, crossover trial. *The Lancet*. 2017;390(10111):2481-2489.

19. Assessment of Clemastine Fumarate as a Remyelinating Agent in Acute Optic Neuritis (ReCOVER).

20. Percie du Sert N, Hurst V, Ahluwalia A, *et al*. The ARRIVE guidelines 2.0: Updated guidelines for reporting animal research. *Journal of Cerebral Blood Flow & Metabolism*. 2020;40(9):1769-1777.

21. Dombeck DA, Harvey CD, Tian L, Looger LL, Tank DW. Functional imaging of hippocampal place cells at cellular resolution during virtual navigation. *Nature neuroscience*. 2010;13(11):1433-1440.

22. Lee JS, Briguglio JJ, Cohen JD, Romani S, Lee AK. The statistical structure of the hippocampal code for space as a function of time, context, and value. *Cell*. 2020;183(3):620-635.e22.

23. Thevenaz P, Ruttimann UE, Unser M. A pyramid approach to subpixel registration based on intensity. *IEEE transactions on image processing*. 1998;7(1):27-41.

24. Stringer C, Wang T, Michaelos M, Pachitariu M. Cellpose: a generalist algorithm for cellular segmentation. *Nature Methods*. 2021;18(1):100-106.

25. Deneux T, Kaszas A, Szalay G, *et al*. Accurate spike estimation from noisy calcium signals for ultrafast three-dimensional imaging of large neuronal populations in vivo. *Nature communications*. 2016;7(1):12190.

26. Sheintuch L, Rubin A, Brande-Eilat N, *et al*. Tracking the same neurons across multiple days in Ca2+ imaging data. *Cell reports*. 2017;21(4):1102-1115.

27. Gibson EM, Purger D, Mount CW, *et al*. Neuronal activity promotes oligodendrogenesis and adaptive myelination in the mammalian brain. *Science*. 2014;344(6183):1252304.

28. Kalincik T, Vivek V, Jokubaitis V, *et al*. Sex as a determinant of relapse incidence and progressive course of multiple sclerosis. *Brain*. 2013;136(12):3609-3617.

29. Villoslada P, Steinman L. New targets and therapeutics for neuroprotection, remyelination and repair in multiple sclerosis. *Expert opinion on investigational drugs*. 2020;29(5):443-459.

30. Mei F, Lehmann-Horn K, Shen Y-AA, *et al*. Accelerated remyelination during inflammatory demyelination prevents axonal loss and improves functional recovery. *Elife*. 2016;5:e18246.